Eur. Phys. J. A **30**, 351–356 (2006)
DOI 10.1140/epja/i2006-10135-4

THE EUROPEAN PHYSICAL JOURNAL A

g-factor of the $9/2^+$ isomeric state in ^{65}Ni from transfer reaction

G. Georgiev[1,2,a], I. Matea[1,3], D.L. Balabanski[4,5,6,7], J.M. Daugas[8], F. de Oliveira Santos[1], S. Franchoo[9], F. Ibrahim[9], F. Le Blanc[9], M. Lewitowicz[1], G. Lo Bianco[6,7], S. Lukyanov[10], V. Meot[8], P. Morel[8], G. Neyens[11], Yu.E. Penionzhkevich[10], A. Saltarelli[6,7], O. Sorlin[9], M. Stanoiu[9], M. Tarisien[8,3], N. Vermeulen[11], D. Verney[9], and D. Yordanov[11]

[1] GANIL, BP 55027, F-14076 Caen Cedex 5, France
[2] CERN, CH-1211 Geneva 23, Switzerland
[3] CENBG, Bordeaux-Gradignant, France
[4] INRNE, Bulgarian Academy of Sciences, BG-1784 Sofia, Bulgaria
[5] University of Sofia, BG-1164 Sofia, Bulgaria
[6] Dipartimento di Fisica, Università di Camerino, 62032 Camerino (MC), Italy
[7] INFN - Perugia, 06123 Perugia, Italy
[8] CEA/DIF/DPTA/PN, BP12, 91680 Bruyères le Châtel, France
[9] IPN, F-91406 Orsay Cedex, France
[10] FLNR-JINR, Department of Physics, 141980 Dubna, Moscow Region, Russia
[11] K.U. Leuven, IKS, Celestijnenlaan 200 D, B-3001 Leuven, Belgium

Received: 24 May 2006 / Revised: 13 October 2006 /
Published online: 28 November 2006 –
Communicated by D. Guerreau

Abstract. We report a measurement of the g-factor of the $I^\pi = 9/2^+$, $t_{1/2} = 22\,\mathrm{ns}$ isomer in ^{65}Ni. The state of interest was populated and spin-oriented using a single-neutron transfer on an enriched ^{64}Ni target. The value, which was obtained, $g(9/2^+, {}^{65m}\mathrm{Ni}) = -0.296(3)$ is well in agreement with the g-factors of the other $9/2^+$ states in the region and with large-basis shell model calculations. The known g-factor of the $9/2^+$ isomer in ^{63}Ni was used in order to verify the strength of the hyperfine field of Ni(Ni) at room temperature.

PACS. 21.10.Ky Electromagnetic moments – 23.20.En Angular distribution and correlation measurements – 25.45.Hi Transfer reactions – 27.50.+e $59 \leq A \leq 89$

1 Introduction

The nuclear magnetic dipole moment is a highly sensitive probe of the single-particle properties of the nuclear wave function. The composition of the magnetic-moment operator, which depends on the proton/neutron character of the valence nucleons as well as their orbital and spin angular momenta, makes possible the identification of the configuration of the state under investigation and provides an insight into the purity of its wave function.

The single-particle properties are expected to be most pronounced in nuclei next to shell closures, for which the extreme single-particle approximation is expected to be valid. This should show up as an observation of the experimental magnetic moments being very close to the Schmidt values. For mid-shell nuclei the higher number of valence nucleons favors collective degrees of freedom and, subsequently, the observed magnetic moments take values away from the Schmidt lines.

With all of this in mind, it is possible to study shell closures when following the experimental magnetic moments of a chain of nuclei in their vicinity. A good example is provided by the $Z = 28$ closed proton shell Ni nuclei. Nickel is the only element in Nature where three doubly magic isotopes (^{48}Ni, ^{56}Ni and ^{78}Ni) are to be found and the magic character of a fourth one (^{68}Ni) is a long-standing discussion (see, *e.g.*, ref. [1] and references therein). Therefore, a study of the magnetic moments in the chain of nickel isotopes can shed more light on the questions of existence and positions of the neutron closed shells.

Here we report a measurement of the gyromagnetic factor ($g = \mu/I$) of the $I^\pi = 9/2^+$ state ($t_{1/2} = 22\,\mathrm{ns}$, $E_x = 1017\,\mathrm{keV}$) in ^{65}Ni which is expected to have a predominant $\nu g_{9/2}$ character. The positive-parity neutron $g_{9/2}$ orbital appears as an intruder in the negative-parity fp shell above $N = 40$ and it clearly has an important im-

[a] *Present address:* CNRS/IN2P3; Université Paris-Sud, CSNSM, UMR8609, ORSAY-Campus, F-91405, France;
e-mail: georgiev@csnsm.in2p3.fr

pact on the structure of the nuclei in the region. It causes the appearance of doubly magic features in ^{68}Ni [2] but it is still questionable whether this is due to a real shell gap at $N = 40$ or it can rather be attributed to the parity change between the g and fp orbitals and neutron superfluidity [3]. No matter what is the underlying mechanism for this effect, it is expected to be localized [4] and an interesting question is how the structure of the nuclei in this region develops when extra proton or neutron particles (or holes) are added. The g-factor of the $9/2^+$ states in ^{63}Ni [5] and ^{67}Ni [6] are already measured and $g(^{63m}\mathrm{Ni}, I^\pi = 9/2^+) = -0.269(3)$ takes a value in agreement with the g-factors of the other $9/2^+$ states in the region, while $|g(^{67m}\mathrm{Ni}, I^\pi = 9/2^+)| = 0.125(6)$ differs significantly from the value expected for a pure neutron $g_{9/2}$ orbital. Thus, a measurement of the $g(^{65m}\mathrm{Ni}, I^\pi = 9/2^+)$ will provide information on the evolution of the structure of the $9/2^+$ $\nu g_{9/2}$ state towards $N = 40$ in the nickel nuclei.

Preliminary results of this work were reported at the NUSTAR 2005 Conference [7].

2 Experiment

The Time-Dependent Perturbed Angular Distribution (TDPAD) method has been applied for the measurement of the gyromagnetic factor of the $I^\pi = 9/2^+$, state in ^{65}Ni. The experiment was performed at the Orsay Tandem, France. The isomeric state was produced and spin-oriented in a (d, p) reaction using a 6 MeV deuteron beam impinging on an enriched ($\geq 95\%$) ^{64}Ni target. The ferromagnetic properties of the Ni target were used in order to obtain a sufficiently high magnetic field for the TDPAD measurement. The details on the determination of the total magnetic field at the nuclear site will be discussed in sect. 2.3.

The γ-ray from the de-excitation of the isomeric state was observed with a pair of Ge and a pair of BaF_2 detectors positioned in a horizontal plane at $\pm 135^\circ$ and $\pm 45^\circ$ with respect to the beam axis. An electromagnet, providing an external magnetic field in vertical direction, was used to orient the internal hyperfine field of the Ni foil, which also served as both a target and a host due to the very low recoil energy of ^{65}Ni nuclei after the (d, p) reaction.

2.1 Experimental method

In a TDPAD experiment the intensities of the de-exciting transitions of an isomeric state are measured at specific angles as a function of time. The applied magnetic field causes the rotation of the nuclear spin-oriented ensemble with a Larmor frequency, $\omega_L = -g\mu_N B/\hbar$, that is directly proportional to the gyromagnetic factor of the isomeric state and the magnetic field at the nuclear site. One can easily derive the g-factor of the state of interest using the standard $R(t)$-function giving the difference in the intensities between two detectors positioned at 90° with respect to each other at a plane perpendicular to the magnetic field, normalized to their sum

$$R(t,\theta,B) = \frac{I(t,\theta,B) - I(t,\theta+\pi/2,B)}{I(t,\theta,B) + I(t,\theta+\pi/2,B)} = \frac{3A_2B_2}{4+A_2B_2}\ \cos\{2(\theta-\omega_L t-\alpha)\}. \quad (1)$$

Here A_2 is the angular-distribution coefficient, B_2 is the orientation parameter and θ is the angle for the first detector with respect to the beam direction, ω_L is the Larmor frequency and α is the angle between the beam direction and the symmetry axis of the spin-oriented ensemble ($\alpha = 0$ for in-beam experiments). In the above expression we take into account only the second-order term and neglect the higher-order terms, because they are usually about an order of magnitude smaller.

In order to minimize any systematic effect one can construct the $R(t)$-function using a single detector, and performing measurements at opposite directions of the magnetic field giving the general expression

$$R(t,\theta,\pm B) = \frac{I(t,\theta,+B) - I(t,\theta,-B)}{I(t,\theta,+B) + I(t,\theta,-B)} = \frac{3A_2B_2\sin 2(\theta-\alpha)\sin(2\omega_L t)}{4+A_2B_2+3A_2B_2\cos 2(\theta-\alpha)\cos(2\omega_L t)}.$$

This brings us to a more complex form of the $R(t)$-function, which is time dependent both in the numerator and in the denominator, and its amplitude depends on the angular position of the detector (θ). After taking into account that our detectors are positioned at $\theta = \pm 45^\circ$ and $\pm 135^\circ$, implying a specific symmetry of the setup, we arrive to

$$R(t,\pm B) = \frac{3A_2B_2}{4+A_2B_2}\ \sin(2\omega_L t), \quad (2)$$

which is practically identical to the $R(t)$-function of eq. (1). The application of the $R(t)$-function with a change of the direction of the magnetic field is quite useful in order to get rid of detector-related effects which might cause systematic errors. However, the positions of the detectors with respect to the nuclear alignment axis should be considered carefully. A shortcoming of this technique is that in order to obtain the same statistical accuracy per field direction per single detector twice longer data-taking time is needed.

2.2 Experimental details

The experiment was performed using a pulsed D beam with an intensity of less than 1 nA, a width of each pulse ~ 2 ns and a period between two pulses of 400 ns. The time structure of the beam was chosen in a way that the period between two pulses is sufficiently long in order to allow the complete decay of the isomeric states before the next pulse arrives. For each event, accepted by the data acquisition, energy and time were recorded. The energy was obtained

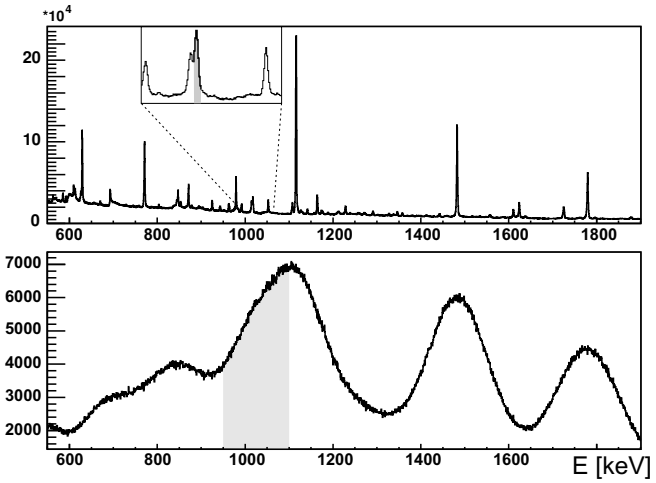

Fig. 1. Typical energy spectrum for a Ge (upper part) and a BaF_2 (lower part) detector. The relevant part with the 1017 keV transition de-exciting the isomeric state of ^{65}Ni is shown as an inset. The shadowed areas show the energy gates used for the $R(t)$-functions.

directly by the amplified signal of the γ-ray detectors. The time was provided by Time-to-Digital Converters (TDC), for which the fast signals from the γ-ray detectors served as a start and the beam pulse was used as a stop. Energy *vs.* time matrices were sorted and analyzed off-line.

A typical energy spectrum revealing the γ-decay of the isomeric state in ^{65}Ni is presented in fig. 1. The 1017 keV γ-line, which is the only transition de-exciting the isomeric state, is sufficiently well separated from the 1014.4 keV γ-rays originating from the ^{27}Al(n, n$'\gamma$) reaction. In the BaF_2 detectors the spectrum is dominated by strong β-decay lines and the isomeric transition cannot be distinguished. Using the shadowed areas, as presented in fig. 1, energy-gated time spectra for the isomeric transition in ^{65}Ni were constructed. The half-life of the isomeric state, which was determined using the sum of the time spectra, was found to be $t_{1/2} = 22(2)$ ns, in agreement with the previously reported value 18.5(7) ns [8]. These time spectra were used in order to construct $R(t)$-functions for all possible combinations of detectors and magnetic-field directions as described above (eq. (1) and eq. (2)).

Since the peak-to-background ratio differs considerably between the Ge and the BaF_2 detectors, the data for each detector pair were analyzed separately. Note that although in the BaF_2 detectors the isomeric γ-ray is practically indistinguishable from the β-decay background, a clear TDPAD pattern is observed in the $R(t)$-functions in this case (see fig. 2). This can be attributed to the fact that the γ-lines from the β-decay background are not time correlated within the beam pulsing period and their angular distribution is practically isotropic. In order to verify that the pattern observed in the $R(t)$-functions from the BaF_2 detectors is indeed originating from the isomeric transition and not any other artificial sources we have constructed another $R(t)$-function, for which the energy gate was set at sufficiently high energy in order to avoid any

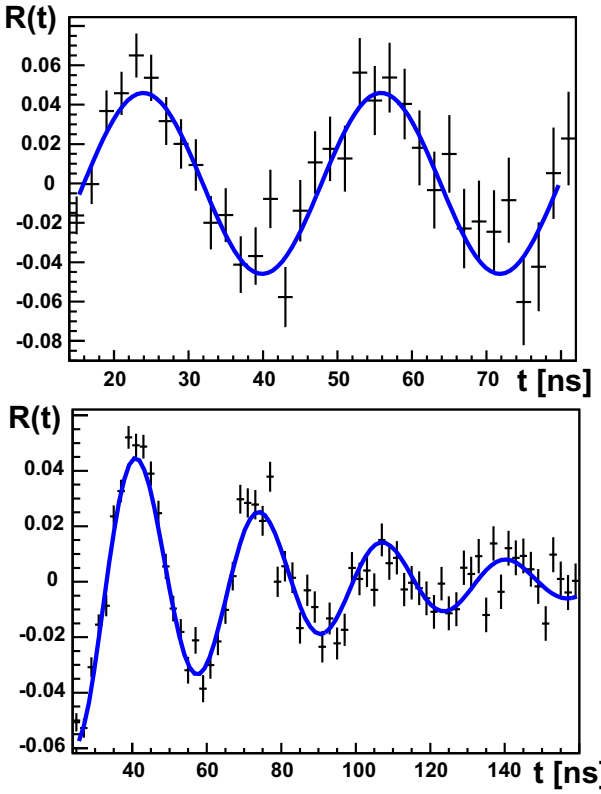

Fig. 2. $R(t)$-functions for the "all together" combination of the Ge (upper part) and BaF_2 (lower part) detectors. See the text for more details.

Table 1. Results from the χ^2 fit to the $R(t)$-functions for all possible detector and field combinations. See the text for more details.

		Ge detectors	BaF_2 detectors
		$g_{exp.}$	$g_{exp.}$
$B\uparrow$ *vs.* $B\downarrow$	det. 1	−0.296(4)	−0.301(4)
	det. 2	−0.301(6)	−0.288(3)
det.1 *vs.* det.2	$B\uparrow$	−0.300(4)	−0.287(3)
	$B\downarrow$	−0.296(5)	−0.298(3)
"all together"		−0.298(3)	−0.293(4)

influence from the isomeric γ-ray. This background $R(t)$-function did not show any sign of TDPAD oscillations, as expected.

The g-factors derived from all possible combinations (see table 1) are consistent within the statistical uncertainty, which gives confidence in the result obtained. The notations used are $B\uparrow$ and $B\downarrow$ for field-up and field-down, "det. 1" denotes the Ge detector at −135° and the BaF_2 detector at 45°, and "det. 2" is the second detector for each pair, respectively.

In order to deduce the value of the g-factor without giving preference to any of the two methods, a slightly different procedure was applied: The time spectrum for det. 1 field-up was added to the time spectrum of det. 2 field-down and further opposed to the sum of det. 1 field-down plus det. 2 field-up. The so-constructed $R(t)$-function has

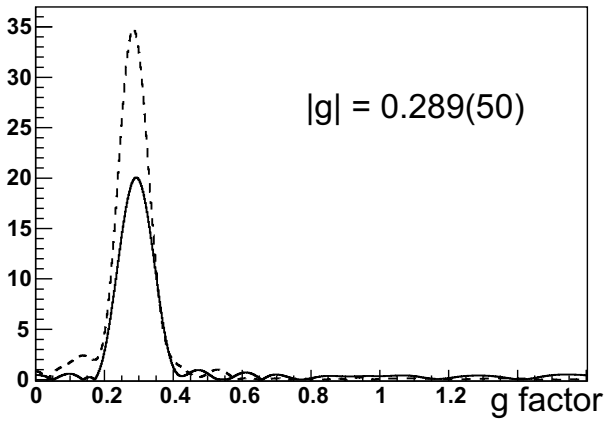

Fig. 3. Results from the Fast Fourier Transform of the $R(t)$-functions for the Ge (full line) and BaF_2 (dashed line) detector pairs. The direct correspondence of the results to the gyromagnetic factors (using the magnetic field as described in sect. 2.3) is shown instead of the standard frequency notations.

the following expression:

$$R(t) = \frac{[I_{det.1}(B\uparrow) + I_{det.2}(B\downarrow)] - [I_{det.1}(B\downarrow) + I_{det.2}(B\uparrow)]}{I_{det.1}(B\uparrow) + I_{det.2}(B\downarrow) + I_{det.1}(B\downarrow) + I_{det.2}(B\uparrow)}.$$

In this manner the whole statistics of the experiment was used without introducing any "double counting", which would appear if the average value of the g-factors of all possible combinations is taken. The results from this procedure are presented in the last row of table 1 ("all together") for the Ge and BaF_2 detector pairs. All g-factors values presented in table 1 are obtained using a magnetic field at the nuclear site, as described in the following section.

The $R(t)$-functions, resulting from the abovementioned procedure, are presented in fig. 2. The amplitude damping, observed in the pattern derived from the BaF_2 detectors is due to the very strong β-decay background contribution in the time spectra. With the decay of the isomeric state the peak-to-total ratio decreases exponentially which causes this artificial behavior. Clearly, no similar trend is observed in the $R(t)$-function from the Ge detectors. This supports the conclusion that no real deorientation effects are observed within the lifetime of the isomeric state.

Finally, the Fourier spectra of the measured $R(t)$-functions were deduced using the fast Fourier transform (FFT). They display a single frequency in the FFT plots, which are presented in fig. 3, very well in agreement with the results from the fits to the $R(t)$-functions.

2.3 Magnetic-field determination

The magnetic field at the nuclear site can be determined as

$$B_{tot.} = B_{hf} - B_{dem.} + B_{ext.}(1 + K), \qquad (3)$$

where B_{hf} is the hyperfine field of the material in which the nuclei are implanted, $B_{dem.}$ is the demagnetization field, $B_{ext.}$ is the externally applied magnetic field and K is the Knight shift.

Two values have been reported for the hyperfine field of nickel in nickel. An NMR measurement of the temperature dependence of the hyperfine field of Ni(Ni) reports $B_{hf} = -6.9505(3)$ T at room temperature [9]. In ref. [10] a value of $B_{hf} = -7.6(1)$ T is determined at liquid-He temperature. The present experiment was performed at room temperature and, therefore, we consider the former value.

The demagnetization field depends on the shape and the sizes of the ferromagnetic host and it is not straightforward to be obtained in a general analytical expression (see, *e.g.*, ref. [11]). For polycrystalline samples with a regular shape the demagnetization field can be presented as

$$B_{dem.} = \mu_0 \hat{D} M, \qquad (4)$$

where μ_0 is the magnetic permeability of vacuum and $\hat{D}$ is the demagnetization tensor. Due to the magnetic isotropy of the sample only the diagonal elements differ from zero. For a thin foil with length a, width b and thickness c; $a \approx b \gg c$, the diagonal elements of $\hat{D}$ can be approximated as

$$D_a \approx \frac{\pi c}{4a}\left[1 - \frac{a-b}{4a} - \frac{3}{16}\left(\frac{a-b}{a}\right)^2\right], \qquad (5)$$

$$D_b \approx \frac{\pi c}{4a}\left[1 + \frac{5(a-b)}{4a} - \frac{21}{16}\left(\frac{a-b}{a}\right)^2\right],$$

$$D_c = 1 - D_a - D_b.$$

Substituting the dimensions of the foils we used during the experiment, $a \sim 10$ mm, $b \sim 10$ mm and $c \sim 100\,\mu$m, and using the intensity of the magnetization value for nickel, $\mu_0 M = 0.64$ T, we can obtain the demagnetization field in each direction, $B_{dem.a} : B_{dem.b} : B_{dem.c} = 5 : 5 : 590$ mT. Therefore the external magnetic field in our thin foils should be reduced by 5 mT.

The external magnetic field we have applied during the experiment was $B_{ext.} = 50.0(5)$ mT where the uncertainty includes also the variations due to the regular change of the direction of the magnetic field. Before the experiment the two targets were annealed at 60% of the nickel melting point. The magnetization measurements, performed on the target foils, have shown that an external magnetic field of about 30 mT was sufficient to fully orient the hyperfine field. Therefore, applying a field, which is more than 50% higher ensures that the saturation hyperfine field is reached during the experiment.

The Knight shift, which one can consider as a correction to the external field, is usually of the order of a few percents. Taking into account previously reported values for a polycrystalline sample at 7 mK ($K(\mathrm{Ni(Ni)}) = 2.8(35) * 10^{-2}$, [12]) even with the expected temperature dependence of the Knight shift its corrections can be completely neglected in the overall estimation of the uncertainty of the magnetic field at the nuclear site.

Thus, the value that was adopted for the magnetic field at the nuclear site is $B_{tot.} = 6.90(2)$ T. All above-mentioned corrections are taken into account together with the possible variations due to a specific treatment of the ferromagnetic hosts.

In addition, a TDPAD measurement on the $I^\pi = 9/2^+$ isomeric state of ^{63}Ni, whose g-factor was known to be $g = -0.269(3)$ [5] was performed. Its half-life was obtained as $t_{1/2} = 10(1)$ ns, in agreement with refs. [5,13], but this value differs considerably from the value adopted in ref. [14], $t_{1/2} = 3.33(21)$ ns. Using the known g-factor of the ^{63m}Ni the magnetic field at the nuclear site can be determined under the same experimental conditions as for the ^{65m}Ni measurement with the only difference that a ^{62}Ni enriched foil was used in the latter measurement. The value obtained, $B_{tot.} = 6.92(9)$ T, is in a perfect agreement with the value determined by the NMR measurement [9]. Since the value $B_{tot.} = 6.90(2)$ T, which is deduced from the NMR measurement, is more precise, it was used to deduce the g-factor of the $9/2^+$ isomer in ^{65}Ni.

3 Results and discussion

The value which was derived for the gyromagnetic factor of the $I^\pi = 9/2^+$ isomeric state in ^{65}Ni is $g_{exp.} = -0.2962\ (24)_{stat.}(9)_{syst.}$. It is obtained as a weighted mean of the Ge and BaF_2 "all together" values (last row of table 1). The statistical error accounts for the uncertainty of the χ^2 fits to the $R(t)$-functions and the systematic one is due to the determination of the magnetic field at the nuclear site.

The experimentally determined gyromagnetic factor $g_{exp.} = -0.2962(25)$ is in a very good agreement with the effective g-factor of the neutron $g_{9/2}$ orbital $g_{eff.}(\nu g_{9/2}) = -0.2976$ (here the standard notation $g_l^{eff} = g_l^{free}$ and $g_s^{eff} = 0.7 g_s^{free}$ is used). In order to obtain a deeper insight into the structure of this state, some more detailed Large-Scale Shell Model (LSSM) calculations were performed, using the m-scheme ANTOINE code [15] of the Strasbourg group.

For this region of nuclei, the valence space has to include the fp proton and neutron shells along with the neutron $\nu g_{9/2}$ orbital. To consider the full proton-neutron $fpg_{9/2}$ valence space with a conventional m-scheme diagonalization is out of the reach for the present days computer capabilities. This valence space can also generate undesired spurious center-of-mass admixtures created by the coupling of $f_{7/2}$ and $g_{9/2}$ orbitals. Therefore, a ^{48}Ca core was considered (more accurately, a ^{40}Ca core with eight frozen neutrons in $\nu f_{7/2}$) with $\pi f_{7/2} p_{3/2} f_{5/2} p_{1/2}$ active orbitals for protons and $\nu p_{3/2} f_{5/2} p_{1/2} g_{9/2}$ active orbitals for neutrons, further on called rg-space. The interaction from ref. [16] was used, which was modified in order to reproduce correctly the position of the $9/2^+$ in ^{61}Fe and ^{63}Ni with a truncation of the valence space allowing for up to a total of $t_{max} = 5$ particle-hole (ph) excitations. It was verified that this modified interaction does not change the results reported in ref. [16]. The number of particle-hole

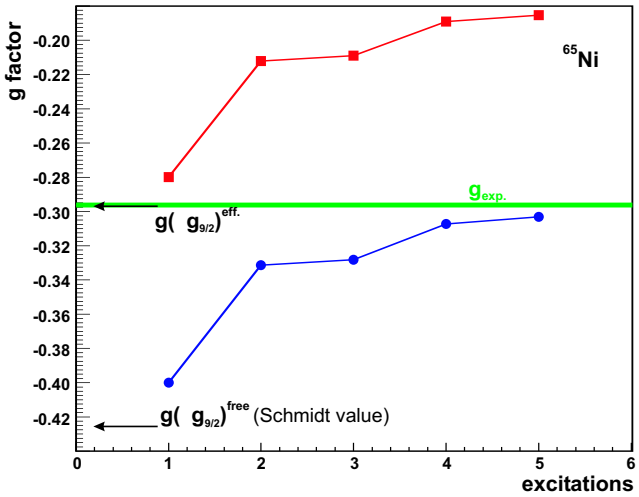

Fig. 4. LSSM calculations for the g-factor of ^{65m}Ni as a function of the allowed particle excitations. The curve with dots represents the values obtained using free-nucleon g-factors, while the effective g-factors values are presented with squares. The straight line presents the experimental value and its width corresponds to the experimental uncertainty. The effective and free-nucleon g-factors of $\nu g_{9/2}$ in the extreme single-particle limit are also presented with arrows.

excitations, t, included either proton excitations from the $f_{7/2}$ orbital to the upper fp orbitals or neutron excitations from the upper fp orbitals to the $g_{9/2}$ orbital. The calculated g-factor as a function of t is shown in fig. 4. At a first glance one can note that the value, obtained using *free*-nucleon g-factors, is getting very close to the experimental value, indicating that the considered valence space might be sufficient to include the necessary correlations for a good reproduction of the magnetic moments of the nickel isotopes.

The results from the LSSM calculations allow the following comments:

- The calculated one ph excitation ($t = 1$) practically corresponds to the case of a single neutron on the $\nu g_{9/2}$ orbit since no proton excitations from the $\pi f_{7/2}$ orbit are allowed. Therefore in this case the deviation of the $g(9/2^+)$ from the Schmidt value of a pure $\nu g_{9/2}$ orbital ($\sim 5\%$) is only due to the neutron excitations within the fp orbitals.
- Allowing two or more ph excitations ($t \geq 2$) means to open the $\pi f_{7/2}$ and $\nu g_{9/2}$ orbitals, which results in a 20% reduction of the isomeric g-factor (see fig. 4). The question which can be put is whether this is due to proton excitations from $\pi f_{7/2}$ or neutron excitations from $\nu g_{9/2}$ orbital.
- The detailed composition of the nuclear wave function indicates that the neutron excitations within the fp orbitals stay practically constant with the increase of t. There are no components with 2 or more neutrons on $g_{9/2}$ that have an individual contribution higher then 1% although such components do exist resulting in a calculated mean occupation number of $\nu g_{9/2}$ of 1.09. The proton excitations from $\pi f_{7/2}$ gradually increase

with t and their contribution ($> 30\%$ for $t = 5$) to the nuclear wave function follows a trend very similar to the trend of the calculated g-factor. The calculated mean occupation of the $\pi f_{7/2}$ orbital is 7.18 for $t = 5$.

All of these allow to conclude that the main reason for the deviation of the $g(^{65m}\mathrm{Ni}, I^\pi = 9/2^+)$ from the Schmidt value of the $\nu g_{9/2}$ orbital should be looked for in the contributions of the proton excitations from the $\pi f_{7/2}$ orbital across the $Z = 28$ shell gap. In order to verify this hypothesis we have repeated the shell model calculations for $t = 1$ and $t = 2$ neglecting the proton contributions to the magnetic moment ($g_s(\pi) = g_l(\pi) = 0$). These calculations have shown that the difference in the g-factor between $t = 1$ and $t = 2$ is less than 0.7%. Therefore, we can conclude that the change in the g-factor as a function of the allowed excitations number t, as illustrated in fig. 4, can be explained by proton excitations only and any other contributions to the effective $M1$ operator cancel out.

LSSM calculations that span over two major shells can reproduce the experimental value using free-nucleon g-factors (note that for the case of ^{65}Ni presented here some of the spin-orbit partners are excluded from the active model space). This shows that the main part of the correlations in the nuclear wave function are already taken into account.

4 Summary

We have performed a g-factor measurement of the $9/2^+$ isomeric state in ^{65}Ni. Due to the very short half-life of the isomer, the only way to populate and study a spin-oriented isomeric ensemble is in transfer reactions. The use of a hyperfine field in a ferromagnetic material allowed the observation of several oscillation periods. The alignment of the nuclear spin ensemble which is created in transfer reactions, although significantly smaller than the alignment which is obtained in fusion-evaporation reactions, was sufficient to observe a clear experimental signature. From the present experiment it was deduced to be of the order of 15%.

This experiment continues the systematic studies of the $9/2^+$ states in the nickel isotopes. The experimental g-factor, compared to LSSM calculations, has revealed significant excitations across the $Z = 28$ shell gap. The theoretical calculations, spanned over more than one major shell, in which free-nucleon g-factors have been used are very well in agreement with the experimental g-factor.

The outcome of this experiment can neither exclude nor confirm the doubly magic character of ^{68}Ni, however, it hints the extremely localized influence of $N = 40$ over the nuclei in the region. This result does not lead to a better understanding of the measured g-factor of the $9/2^+$ isomeric state in ^{67}Ni [6], which still remains a puzzle. More experimental data on the g-factors of the nickel isotopes above $N = 40$ and right at ^{68}Ni are needed for the understanding of the structure in the region.

We are grateful to the Orsay Tandem engineers for providing us the beam in stable conditions, to the IN2P3/EPSRC French/UK loan pool for providing the Ge detectors, to J. Meersschaut for performing the magnetization measurements of the targets and to M. Hass for providing the electromagnet. This work has been partially supported by the INTAS project No. 00-0463, the IUAP project P5/07 of the Belgian Science Policy Office and by the Bulgarian National Science Fund under contract VUF06/05.

References

1. H. Grawe, M. Lewitowicz, Nucl. Phys. A **693**, 116 (2001).
2. R. Broda *et al.*, Phys. Rev. Lett. **74**, 868 (1995).
3. O. Sorlin *et al.*, Phys. Rev. Lett. **88**, 092501 (2002).
4. H. Grawe *et al.*, Eur. Phys. J. A **25**, 357 (2005).
5. W. Müller *et al.*, Phys. Rev. B **40**, 7633 (1989).
6. G. Georgiev *et al.*, J. Phys. G **28**, 2993 (2002).
7. G. Georgiev *et al.*, J. Phys. G **31**, S1439 (2005).
8. J. Blons *et al.*, Nucl. Phys. A **582**, 296 (1995).
9. P.C. Riedi, Phys. Rev. B **15**, 5197 (1977).
10. K. Krane, Hyperfine Interact. **15/16**, 1069 (1983).
11. S. Chikazumi, *Physics of Ferromagnetism*, Int. Ser. Monogr. Phys., No. **94** (Clarendon Press, Oxford, 1997).
12. T. Ohtsubo *et al.*, Phys. Rev. C **54**, 554 (1996).
13. T. Ishii *et al.*, Nucl. Instrum. Methods Phys. Res. A **395**, 210 (1997).
14. R. Firestone, in *Table of Isotopes*, edited by V. Shirley, C. Baglin, S. Chu, J. Zipkin, 8th edition (John Wiley and Sons, Inc., New York, 1996).
15. E. Caurier, Shell model code ANTOINE, 1989-2002, IReS, Strasbourg.
16. E. Caurier, F. Nowacki, A. Poves, Eur. Phys. J. A **15**, 145 (2002).